APPARATUS AND INSTRUMENTATION DESIGN FOR

INVESTIGATION OF HYPERTHERMAL- AND

LOW-ENERGY SURFACE IMPACT

CURRENT PRODUCTION

A Thesis

Presented to

the Graduate School of

Clemson University

In Partial Fulfillment

of the Requirements for the Degree

Master of Science

Physics

---

by

Stephen Andrew Moody

August 2006

Advisor: Dr. Chad E. Sosolik

ABSTRACT

Recent experiments in the field of surface science have demonstrated electron-hole pair production due to thermal energy neutral particle adsorption on a thin-film Schottky diode. We seek to extend these experiments into higher energy regimes using the hyperthermal- and low-energy ion beamline installed in the Sosolik Research Lab at Clemson University. However, in order to perform this experiment a number of apparatus and instrumentation changes must be made to the beamline system.

This thesis begins by presenting the characteristics and capabilities of the beamline instrument, followed by a brief survey of previous work in Schottky diode "chemicurrent" detection. Several results likely to follow from the extension of this experiment to energetic ion beams are postulated, and the changes necessary to acquire this capability and the challenges involved in accomplishing those changes are discussed.

The final chapters present a narrative of the work completed under the scope of this project to enable hyperthermal Schottky diode scattering experiments: 1) design and construction of a new sample transfer apparatus; 2) instrumentation and associated programming changes to improve the efficiency of beamline operation. Logic-flow diagrams corresponding to the discussed programs are contained in an appendix.

ACKNOWLEDGEMENTS

TABLE OF CONTENTS

Table of Contents (Continued)

LIST OF FIGURES

CHAPTER 1

INTRODUCTION AND EXPERIMENTAL BACKGROUND

Introduction

All work for this project was done relating to a single instrument, a low/hyperthermal energy ion beamline installed in the Sosolik Research Laboratory at Clemson University. While the instrument was originally designed and operated at Cornell University, it was transferred to Clemson and the Sosolik Research Group in the spring of 2004.

Comprehension of the scope and purpose of this project requires an understanding of 1) the design and capability of the beamline instrument; 2) the anticipated experiment. These two points will be explored in that order in this chapter, concluding with a short summary of the work to follow in chapters 2 and 3 discussing the motivations and scope of work undertaken.

Beamline Instrument Design

As noted above, the instrument is categorized as a hyperthermal-to-low energy beamline, operating at ultrahigh vacuum (UHV) and capable of operation using a wide variety of gas and solid-state (typically alkali or occasionally alkali-earth metals) sources. The hyperthermal regime is defined loosely to be the regime of single particle energies above thermal energies (< 1 eV) but lower than approximately 1 keV. The low energy regime starts where the hyperthermal regime leaves off and continues to ~ 10 keV [1]. As Figure 1.1 shows, these regimes are particularly important because it is in these

regimes that kinetic effects dominate particle-surface interactions. At lower (thermal) energies the interaction is dominated by adsorption effects, while at very high energies complex phenomena such as embedding result. Therefore, the low and hyperthermal energy regimes, with scattering as the dominant phenomenon, generate the most directly observable information about complex surface-particle interactions. This information is particularly useful to characterize a broad range of chemical reactions, and in particular the set of reactions occurring in the presence of a surface catalyst.
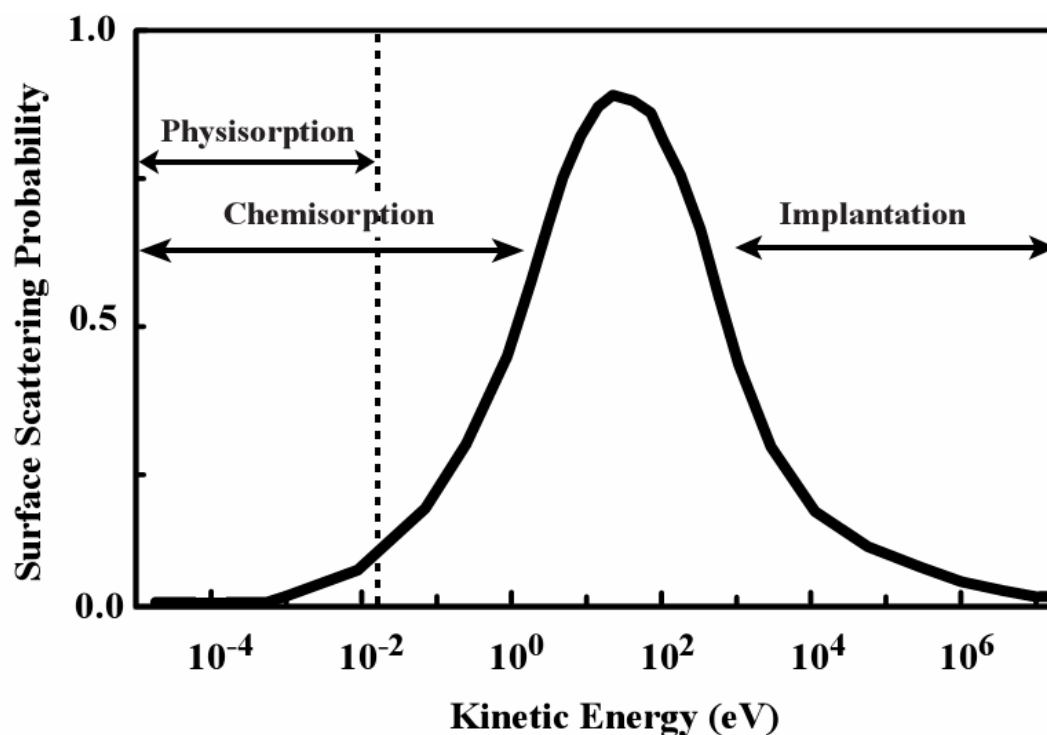
Figure 1.1   Kinetic energy regimes for single-particle incident scattering. The regimes considered here are characterized by incident particle scattering events of approximately the given magnitudes: thermal, $E < 1$ eV; hyperthermal, 1 eV $< E < 1$ keV; low, 1 keV $< E < 10$ keV. It is important to note that these regimes are approximate and useful as guidelines only. Note that scattering probability is peaked in the hyperthermal region [2].

.

The instrument utilizes a beam of ions for two primary reasons. First, the need to generate, characterize, focus, transport, and accelerate a particle beam at above-thermal energies requires that the constituent particles be ionized. Generation of a particle beam at thermal energies is possible through use of a pressurized source or with a hot aperture calibrated to produce an energy distribution about the required energy. In higher-energy regimes this breaks down, since the pressures required become difficult to achieve while maintaining controllable chamber pressure. In addition, the hot aperture begins to ionize the constituent particles above a certain temperature. Energy and species characterization is also quite difficult using neutral particle beams since energy spectra are generally quite broadly spaced and elemental or isotopic impurities cannot be differentiated from the constituent population. True beam focusing and efficient transport of neutral particles is not possible using typical sources and can only be approximated using highly collimated transport sections, resulting in high-loss transport. Finally, acceleration is also not generally possible, as neutral particles present no physical properties which can be used to do work.

All of these problems become trivial using an ionizing beam source and appropriately designed charged-particle optics and characterization instrumentation. Figure 1.2 shows the plan layout of the ion beam instrument with relevant components noted.

A wide variety of beam species are available, using a hot-filament source for gas beams or aluminosilicate source for alkali beams. The produced beam is energy and species characterized with a high degree of precision using a Wien filter [3, 4] and spherical monochromator [5], which narrows the beam energy spread to $\Delta E/E \sim 1\%$ [6].

The beam is focused for transport and accelerated to voltage at various stages of the instrument using a series of electrostatic lens elements [7].
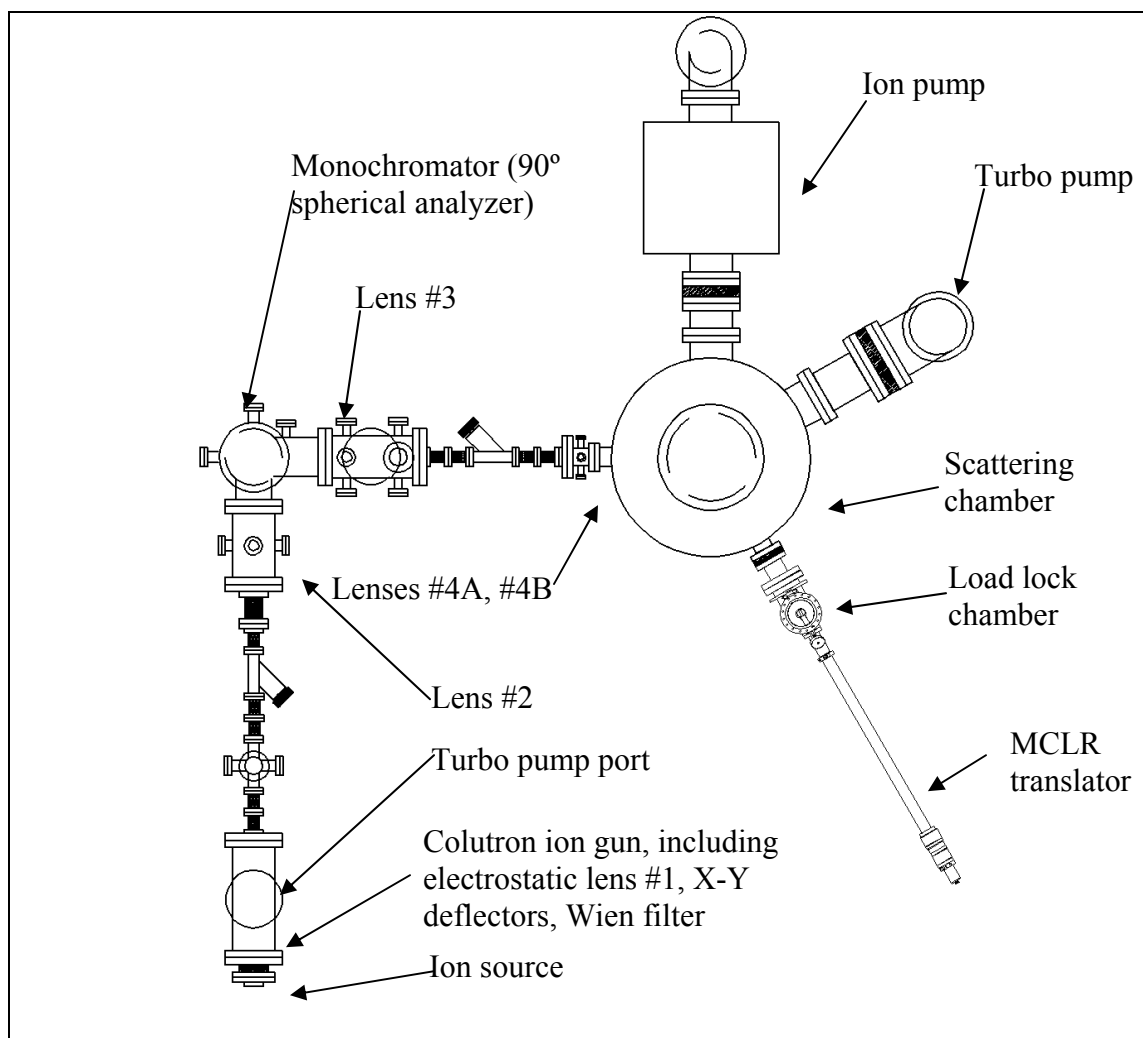
Figure 1.2   Plan view of beamline instrument. Key components, including Einzel lenses, filtering apparatus, vacuum pumps, scattering chamber, and newly installed load-lock/linear translator are shown.

While using an ionized beam greatly simplifies many of the challenges involved in producing a reliable, well-characterized beam, the use of an ionized beam also allows exploration of charge transfer and spin-dependent surface effects. Although sometimes it may be desirable to neutralize the incident beam before striking a surface, in general

these effects provide another useful parameter and several previous studies utilizing this instrument have dealt with these effects specifically.

Schottky Diode Experiment

The unique capabilities of this ion beam instrument make it an intriguing tool for exploring a recently active field of study. While electron-hole pair creation has long been assumed to be one of the primary means of energy exchange at surfaces (see Figure 1.3), until recent experiments by Nienhaus, et al. that mechanism had not been studied via direct observation.
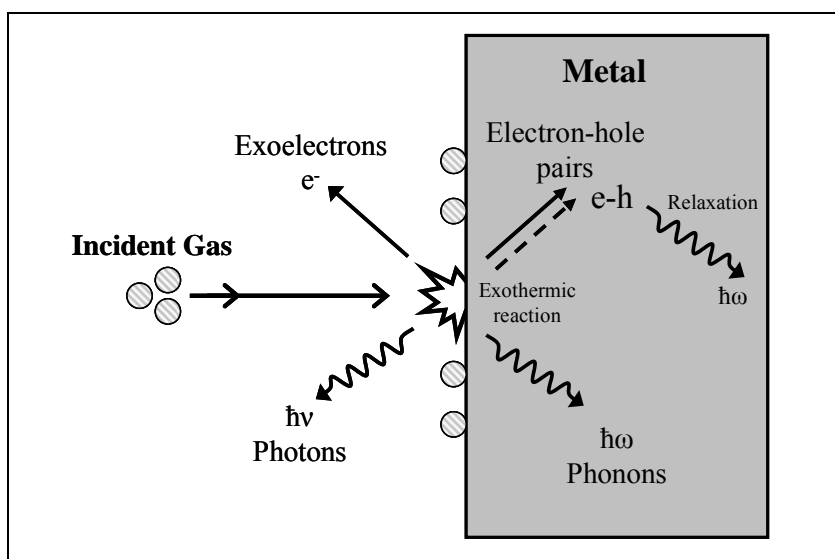
Figure 1.3   Survey of energy exchange mechanisms in surface interactions. Electron-hole pair creation is an important pathway but has been difficult to detect directly [8].

Background and Survey of Previous Work

Recent groundbreaking experiments [9, 10] have directly measured electron-hole pair creation due to neutral particle surface impact events in the form of a "chemicurrent" passing through a metal thin film rectifying (Schottky) diode. A basic Schottky diode device consists of a thin metal film (often Ag, Au, Cu, or Ti) deposited on a doped

semiconductor with some way of measuring current between the thin film and outer edge of the semiconductor. Figure 1.4 illustrates the general design as implemented in these previous experiments.
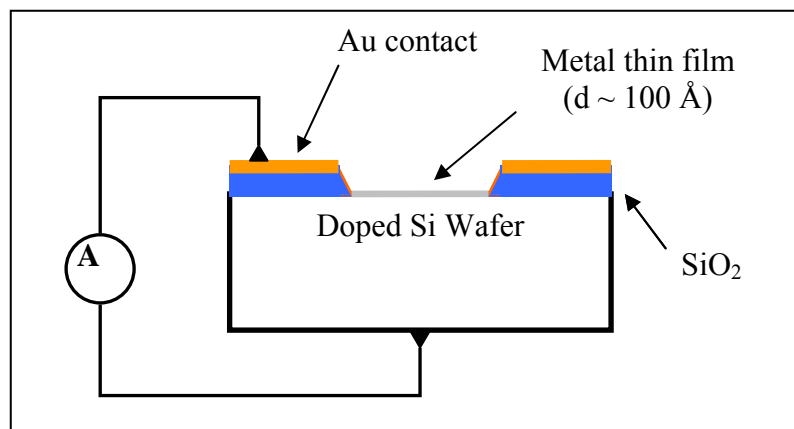
Figure 1.4   Schottky diode design for molecular scattering experiments. The incident molecular beam strikes the metal thin film, allowing a "chemicurrent" to be measured between the front and back contacts [11].

An electron-hole pair consists of a "hot," or energized, electron excited above the Fermi level and leaving behind a "hot" hole in the conduction band at an energy below the Fermi level. Due to their increased energies both the electron and hole are transported ballistically through the material. In bulk materials scattering and coupling effects reduce the pair's energy, eventually causing them to recombine at the Fermi level and disappear. While theoretically detectable, under laboratory conditions this recombination time (or equivalently the e-h pair's mean free path) is so short as to make the process undetectable in practice.

To surmount this detection limitation a Schottky diode utilizes a thin film rectifying contact to make it energetically impossible for electrons (or holes, depending on the diode type) transported across the barrier from returning to recombine with their paired component, thus preventing e-h pair recombination. After a large number of such

events a bulk charge difference builds up across the barrier such that if a circuit is connected between the opposite sides of the device the resulting net flow of electrons would be significant enough to be detectable as current. Figure 1.5 shows an example of the n-type semiconductor case, in which an electron is excited above the Fermi level and ballistically transported into the conduction band of the semiconductor. The electron quickly loses the energy required to return to the metal layer and is then constrained within the conduction band by the energy band gap shifting near the interface.
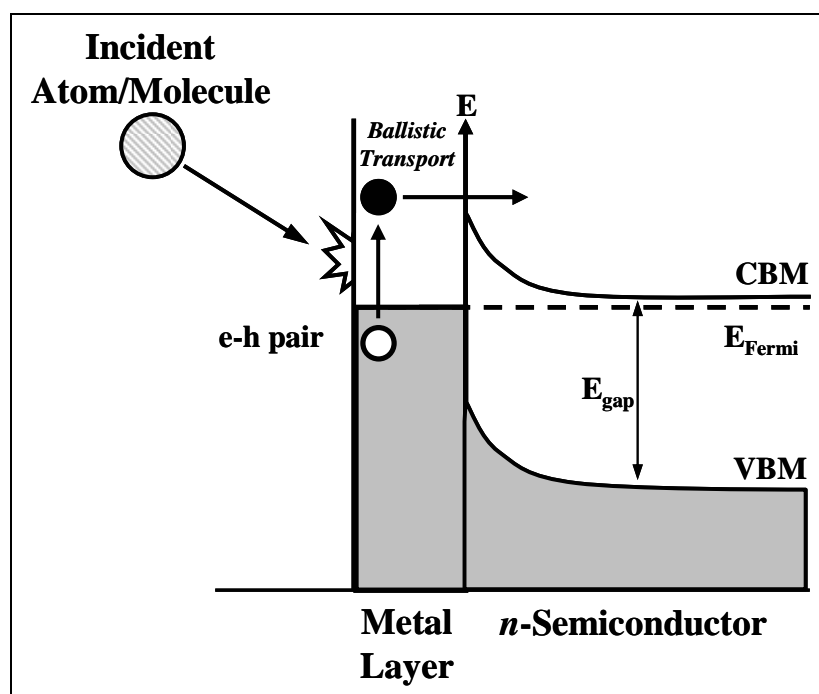
Figure 1.5   Basic operating principle behind n-type Schottky diode device. The p-type would be similar except that the *hole* would cross the barrier below the Fermi level and into the semiconductor valence band [12].

Studies into device optimization so far have shown that measured current depends very sensitively on film thickness, not surprisingly dropping off quite rapidly once the film thickness exceeded the electron mean free path for the film material [13]. Optimal devices used up to this point for the detection of thermal neutral species have generated

chemicurrent of magnitude < 10 nA using film thicknesses of 10 nm or less [multiple sources].

The introductory studies in chemicurrent detection have all used neutral gas species at thermal (< 1 eV) energies, where, as Figure 1.1 shows, the primary source of energy for electron-hole pair creation in the thermal regime is surface adsorption, as incident molecules form a stable bond with the surface and release the excess energy to the surroundings.

Because adsorption (particularly chemisorption) is the dominant energy source the current detected came to be known as "chemicurrent." Although for the energies considered here chemisorption is not the dominant source of energy transfer the term "chemicurrent" will be used throughout this paper to refer to a measurable current due to bulk electron-hole pair creation by some mechanism of surface energy exchange, whether chemical or kinetic.

One distinctive feature of thermal energy incidence experiments and the accompanying predominance of adsorption effects is the tendency of the adsorbing surface to eventually become saturated such that equilibrium is reached between surface adsorption and desorption rates. Gratifyingly this saturation effect manifests itself quite clearly as a distinctive current decay profile as shown in Figure 1.6. The chemicurrent produced starts abruptly when the beam is introduced, decreases exponentially as a function of time, and then terminates abruptly when the beam is shut off.
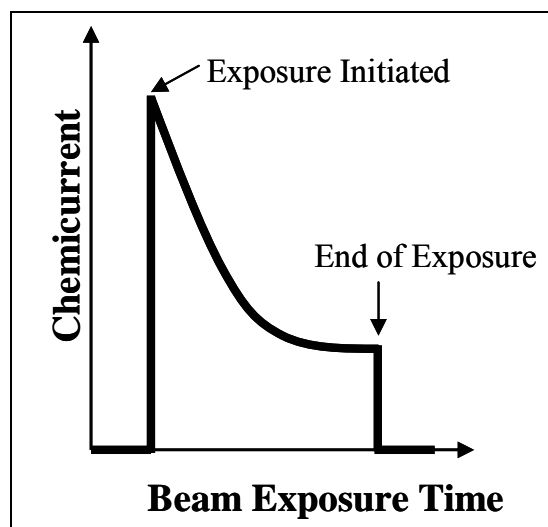
Figure 1.6   Typical chemicurrent vs. exposure time profile. Chemicurrent decay due to surface saturation effects is well illustrated [14].

In addition to being sensitive to exposure time, the chemicurrent profile has been shown to depend on several other parameters consistent with the current understanding of chemicurrent production. These parameters include variation in molecular species, diode semiconductor type (n-type or p-type), beam flux, thin film composition, and even isotopic species.

Extension to Higher-Energy Regimes Using Ion Beam Instrument

The current research goal for the beamline instrument is to extend the chemicurrent sensor results obtained using thermal neutral beams into the low and hyperthermal energy regimes. In doing so it is important to gain an understanding of how the differences between the two experiments are likely to affect the results obtained.

Several differences are immediately apparent. The dominant mechanisms for particle-surface interactions in the different regimes are significant. As mentioned previously, particle-surface interaction is dominated by adsorption effects for thermal energies and by kinetic effects in the hyperthermal and low energy regimes. Accordingly

the chemicurrent profile shown in Figure 1.6 is likely characteristic only for thermal incidence measurements with higher energy profiles exhibiting significantly less-pronounced decay.

Although the particle flux is approximately comparable for the two different cases, it is also likely that the higher-energy case would yield higher overall chemicurrent densities, since the incident particles each carry higher energy. This could result both from the incident particle event imparting more energy to each excited electron and from more electrons being excited for each incident particle. In either case a greater number of electrons would clear the Schottky barrier and the chemicurrent measured would be larger.

Another consequence of the likelihood of higher energies for each electron-hole pair is that thicker films would be more sensitive to chemicurrent than before, since the electron mean free path is dependent on the electron energy. In fact, thicker films may even become necessary to preserve adequate film thickness because of increased sputtering probability at the higher beam energies involved.

The largest area of uncertainty in conducting this experiment involves estimating beforehand what effect the beam's charge state will have on chemicurrent production. Although neutralizing the beam inside the scattering chamber before reaching the Schottky diode sample does not appear to be workable using the present configuration, by carefully choosing the beam and film species it is possible to ensure either very low or very high ion neutralization probabilities after the sample scattering event. The possible effects of ion neutralization "current", electronic heating, and other probabilistic charge dependent effects on surface electronic structure and overall chemicurrent production are

unclear at this point. This is an important question to be considered for future work, possibly to be explored concurrently with preparation for the initial experiment itself.

<p style="text-align: center;">Scope of Work</p>

The beamline instrument was originally designed to facilitate alkali or gas ion scattering off metal crystal surfaces [15], and while the beam species used have varied from experiment to experiment, the available scattering samples have been limited to a small selection of "hat" style metal-crystal samples, with copper and silver being most commonly used. The system was also restricted by the difficulty required to change samples, with the result being that the same sample was often used for months or even years at a time.

One of the primary goals of this work is to increase the sample versatility of the ion beamline, with the primary purpose being to make the experiment outlined above feasible. This involves two separate but related aims: 1) retrofit the manipulator/sample holder design to be able to accommodate rectangular diode samples; 2) make the necessary changes to the sample holder design and the scattering chamber to enable quick sample turnaround. Chapter 2 discusses the design that has been implemented to simultaneously accomplish both aims.

The second primary goal of this work is improve daily operational efficiency for the beamline by designing LabView programs to provide transparent, interactive automation capability for several key processes. Chapter 3 discusses the three main automation applications and sketches the solutions implemented in each case.

CHAPTER 2

SAMPLE HOLDER AND TRANSFER SYSTEM

Introduction

In order to increase the versatility of the ion beamline's scattering chamber, and in particular to facilitate the conduct of the proposed Schottky diode experiment as outlined in Chapter 1, the project required design of a new sample transfer/load lock system with capability to seamlessly transfer samples under vacuum on a carrier specifically designed to provide the enhanced characterization and measurement capability required. The system as nearly completed consists of the following: 1) a sample dock that retrofits the previous sample mounting system of the existing XYZ-translator/manipulator and meets the physical constraints of the system; 2) a sample holder incorporating the necessary electronics contacts as well as intrinsic heating and cooling capabilities; and 3) a vacuum-isolatable load lock/magnetically-coupled linear translator system for transfer and mounting of the new sample holder design.

All of the components mentioned above were custom-designed for our particular requirements: the sample holder/dock stage was designed in AutoCAD using 3D modeling and fabricated by the departmental machine shop, while the load lock/linear translator package was supplied to specification by a third-party vendor. The remainder of this chapter is devoted to discussion of the specification, design, and procurement process for this upgrade, with the major design elements discussed previously divided into separate sections.

Sample Holder

The basic design approach taken for the sample holder assembly, which includes the sample, contacts, heating/cooling capability, and mechanical securing hardware, was to separate the sample and its associated heating and cooling components from the problem of securing the assembly and providing electrical contact to the sample dock. As such the accommodations for the sample and associated components were incorporated into a discrete module which will henceforth be referred to as the sample mount, while the components needed to provide electronic connectivity and secure the sample holder assembly to the sample dock were combined in a separately designed module, known as the sample carrier. The sample mount and sample carrier could then be fastened together to form the complete sample holder device. In addition to making the design process simpler, this approach also has the advantage of allowing a single unified sample carrier design for a variety of possible sample types and shapes.

Sample Carrier Module

The design for the sample carrier module was considered first. Basic requirements included providing connectivity for at least six contacts from sample mount to sample dock while capable of quick sample turnaround at high vacuum. To accomplish this a design consisting of a set of three stacked, rotationally staggered rings that couple to matching hooks on the sample dock was used to provide connectivity, with each split to give a total of six electrical contacts on the sample carrier. A front sample transfer ring designed to couple to a matching sample transfer claw (discussed at the end of this chapter) is stacked on top of the three contact rings to provide rapid sample transfer capability. The four levels are electrically isolated from each other using hollow

alumina spacers. The entire assembly is fastened using lengths of threaded rod passed through the alumina spacers and secured with a hex nut on each end. Figure 2.1 shows the design and primary components of the sample carrier (with no sample or sample mount shown).
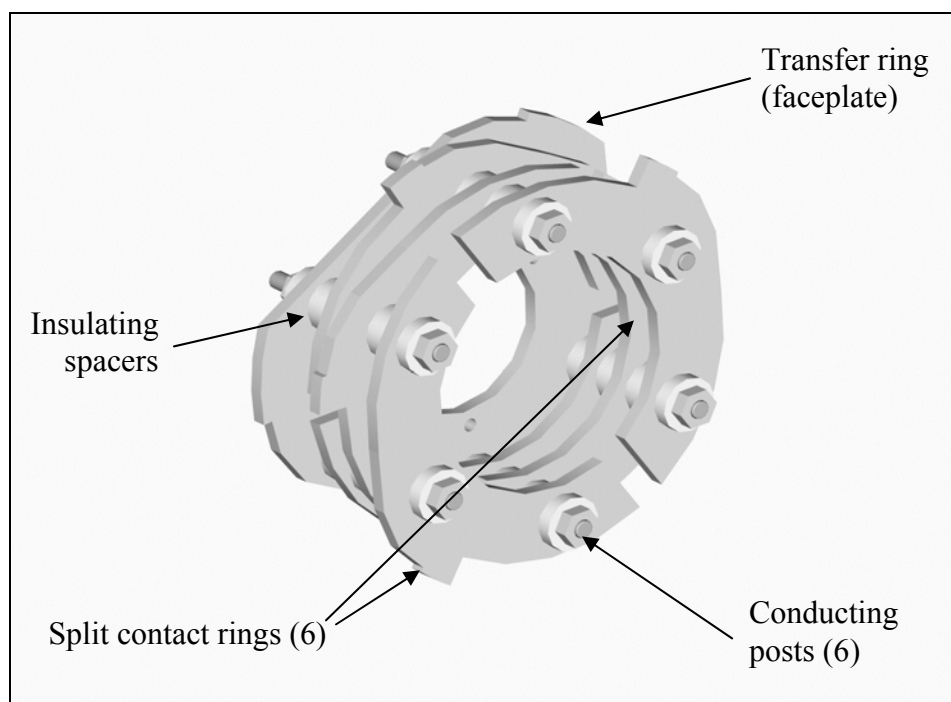
Figure 2.1   Sample carrier back view, without sample holder assembly.

Sample Mount Module

The sample mount had to be versatile enough to allow access for heating and cooling the sample. The same basic design also needed to be able to accommodate both rectangular cleaved silicon-type samples and circular hat-type metal crystal samples. The dimensions for metal crystal samples are already well established, so the new design needed to be able to incorporate those samples without modification. However, the basic design consists of a set of rings designed to be bolted to the face of the sample carrier along with the actual sample retaining piece, which can be interchanged

depending on the sample type. See Figure 2.2 for a diagram of the sample mount as designed for a standard hat-type copper crystal sample.
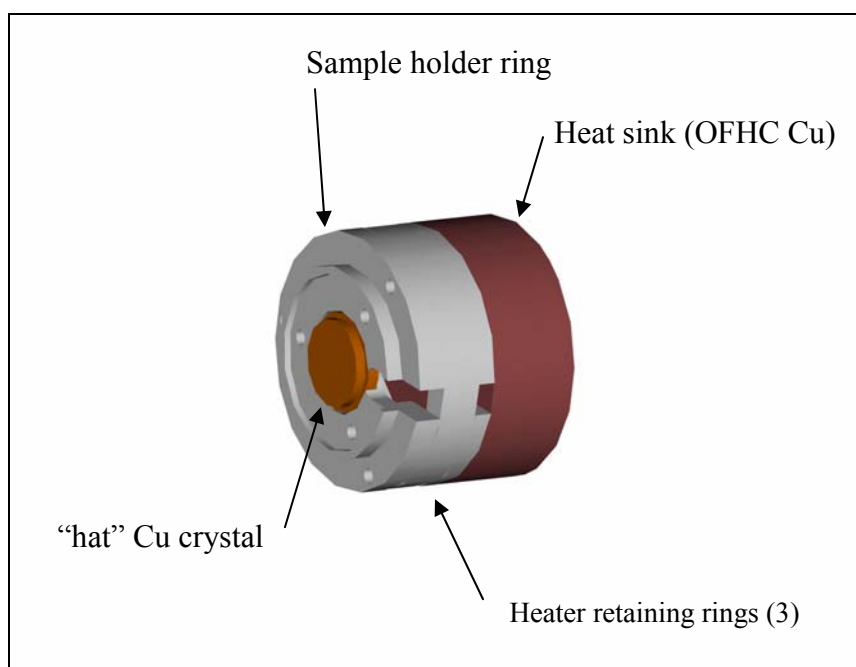
Figure 2.2   Example sample mount configuration for "hat"-type metal crystal sample. Heater rings and OFHC heat sink are shown.

There are several other possible configurations. The sample mount assembly for use in the future with rectangular diode samples will need to be able to electrically isolate the sample from the sample carrier, which the standard sample does not require. This design is not complete since diode dimensions have yet to be determined, but it would presumably incorporate alumina/Macor® spacing rings between the conducting rings in order to accomplish that effect, in much the same way as the individual rings of the sample carrier are electrically isolated from each other.

As an example of a configured sample carrier/holder system, Figure 2.3 shows the standard sample carrier with the sample mount shown in Figure 2.2 installed.

Face contacts (6)

Sample carrier

Sample mount
With sample
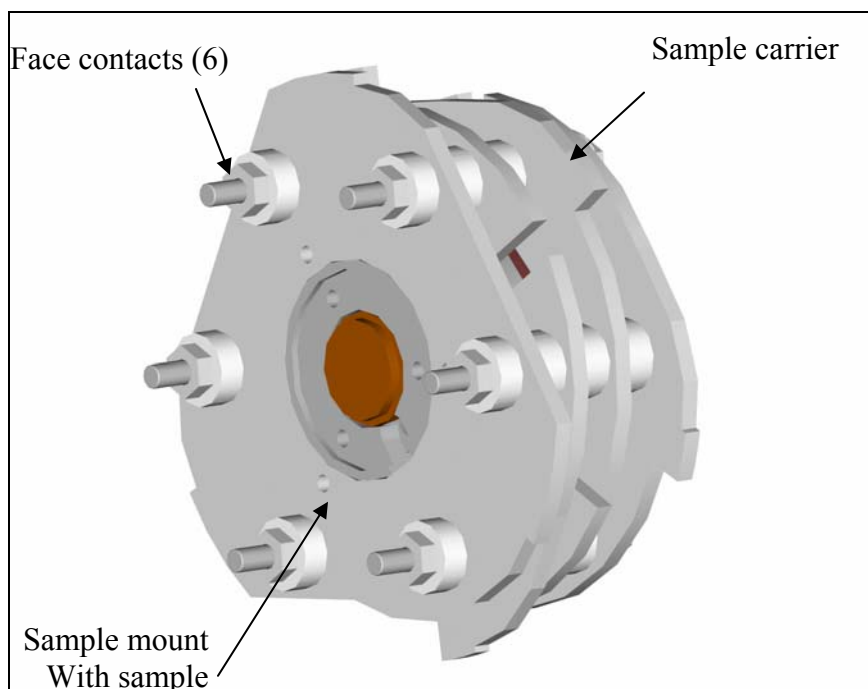
Figure 2.3   Front view of sample holder assembly. Shown are front of sample carrier faceplate and installed locations of sample carrier and sample mount.

In order to provide the ability to monitor and control the sample temperature an integrated heater and external cooling system was implemented. The cooling stage operates via heat conduction through the copper body of the sample dock (described below) as heat is transferred away from the sample via 1/8" flat copper braid strung from the (existing) cooling Dewar mounted alongside the manipulator [16]. In order to cool the sample liquid nitrogen is circulated through the Dewar.

The heater from the previous design was reused in the interest of saving design and implementation time and the sample holder then designed with those size parameters in mind. The heater is integrated into the system via a set of hollow rings designed to hold the heater module close to the back of the sample without making contact with the sample to provide optimum heating qualities without the possibility of damaging the sample or apparatus.

In order to monitor sample temperature set points during heating and cooling cycles it is also necessary to incorporate a thermocouple into the sample mount design. The thermocouple used is of the alumel-chromel type, and measures the sample's front-side temperature via a slot built into the sample holder.

Electrical contacts for both the heater and thermocouple come from the sample dock via the set of staggered rings described previously. This requires a total of four contacts, leaving two contacts for sample sensing or characterization. However, since the heater, thermocouple, and sample contacts are unlikely to ever require simultaneous use the current design should remain robust enough to allow future experiments requiring more than two sample contacts.

Sample Dock

The sample dock was designed in tandem with the sample carrier and was likewise required to be capable of incorporating six sample contacts since the sample carrier module interfaces directly with the hook-contacts on the sample dock. The original manipulator head was quite versatile and would have required significant effort to redesign adequately, so instead the new dock was designed to be dimensionally consistent with the constraints of the original design (although this was not always possible—see 'Redesign' section below). The manipulator allows for six total degrees of freedom (XYZ translation, X-, Y-rotation, tilt). Translation is the simplest, being accomplished using standard linear translation stages to translate the entire manipulator assembly. Rotation about the vertical axis is also accomplished via rotation of the entire assembly, while a worm gear mounted on the manipulator head engages the back securing plate of the sample dock to enable sample rotation along the axis perpendicular

to the sample (X). Finally, a cable tensioning system accessed via an external screwdriver mounted at the top of the manipulator shaft provides capability to tilt the entire manipulator head a few degrees each direction. Figure 2.4 shows the sample dock arrangement as installed in the body of the manipulator and the available rotational degrees of freedom.
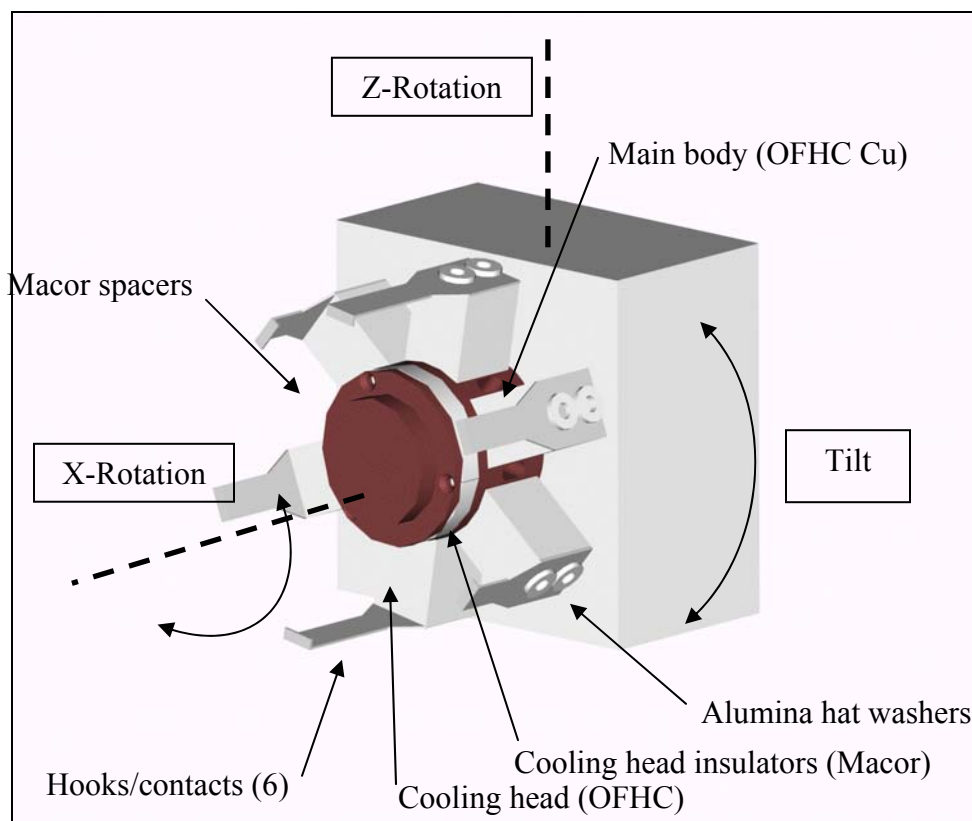
Figure 2.4   Diagram of sample dock. Key exterior parts and available rotational degrees of freedom are labeled.

Since the sample dock needs to fit within the cylindrical bounds provided by the previous design, the foundation of the sample dock is a machined cylinder of oxygen-free, high-conductivity (OFHC) copper of high purity obtained from McMaster-Carr Supply Co. with the appropriate outer diameter to fit within the previously allowed dimension. Copper was chosen because of its high thermal conductivity, while the

specific alloy is used because of its favorable outgassing characteristics in vacuum, particularly when heated [17]. The cylinder interior is cut to a hollow profile as described previously to provide a conduit to the sample carrier for electrical contacts and cooling braid. In order to save space and prevent shorting issues between the cooling braid and electrical contacts, the copper cooling braid is mounted in slots machined in the interior diameter of the dock body.

In order to accomplish the securing of the sample carrier to the dock a system of securing hooks was implemented. The hooks are staggered at three levels with two hooks on each level but on opposite sides of the dock body. This allows each of the six hooks to engage a different ring, and since at each level of the sample carrier the rings are split so that each half-ring is electrically isolated from all the others each of the six hooks engaged a unique split ring so that mechanical docking and electrical contact requirements were met simultaneously. In addition, since the rings (and hence the hooks) are to serve as electrical contacts to the sample front plate, the hooks had to be individually electrically isolated. This was achieved via the use of machined Macor spacers with thru holes drilled in them such that the hooks could be secured to the dock body via machine screws threaded into radial tapped holes in the dock body while still being electrically isolated from the dock and from each other. The hooks were in turn isolated from the machine screws by the use of Alumina hat washers obtained from McAllister Technical Services, Coeur d'Alene, Idaho.

Figure 2.4, a diagram of the docking system, shows how the design met both the mechanical and electrical requirements. The design also allows the sample to be secured redundantly since secure docking of the sample carrier does not require all six hooks to

be securely fastened at once. Using this sequence of hardware it was possible to assemble a docking system that met our requirements both in providing a sufficient number of electrical contacts as well as being mechanically robust enough to allow effective, stable sample docking.

Sample Transfer System

Load Lock/Magnetically Coupled Linear-Rotary Translator

The final component of the completed, operational system is the load lock/linear translator system. Without the versatility to be able to transfer samples quickly in vacuum, the proposed Schottky diode experiment, which requires multiple tests using diodes of varying parameters, would not have been feasible. The most rapid and inexpensive method of procuring such a system was to purchase one off-the-shelf from one of the many vacuum projects vendors in the industry. Because such systems are readily available, the components of the sample transfer system discussed previously were designed to require only linear and rotary translation to complete the sample transfer cycle.

The requirements for the mounting port also need to be taken into consideration. To provide adequate clearance for the sample carrier design, the inside dimension for flanges and tubing in the transfer system needs to be slightly larger than the sample carrier's outer dimension of 2.0". A total inside diameter of 2.25" is therefore adequate to provide clearance for the sample transfer head while avoiding friction or interference in the event that the sample carrier or transfer rod is slightly misaligned.

The chosen mounting port needs to be on the lower level for proper vertical alignment with the sample dock position. A survey of available chamber ports found an

unused 4-½" chamber port (with inside dimension of 2.41") to meet requirements. Competitive quotes were obtained from a number of vacuum firms, and a solution provided by Thermionics Inc., of Port Townsend, WA was contracted, delivered, and installed. See Figure 2.5 for a schematic view of the purchased system. Figure 1.2 shows the general location of the transfer system relative to the rest of the instrument.
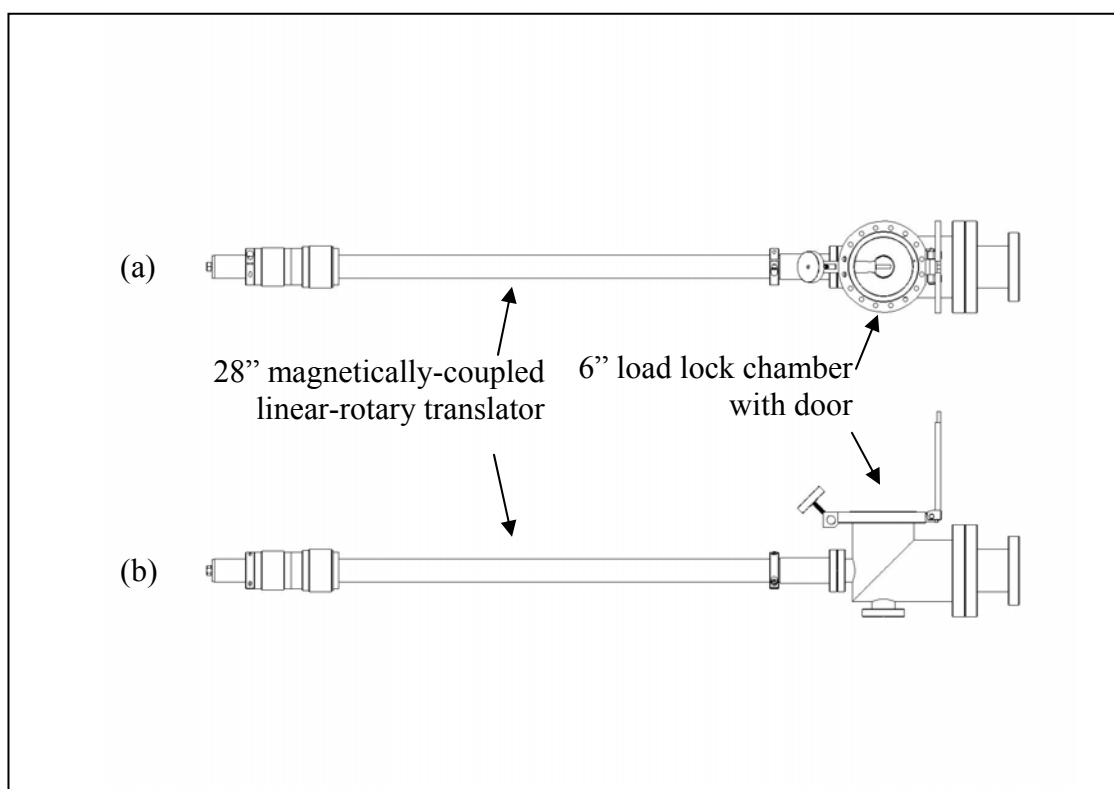
Figure 2.5   Sample transfer system. Top (a) and side views (b) of 28" magnetically-coupled linear-rotary translator (MCLR) with 6" load lock chamber and 6" x 4½" adapter.

Sample Transfer Tool

The final step was to design and construct a "claw" attachment for the linear translator shaft that would securely grasp the sample and enable us to transport the sample carrier securely between the load lock chamber and the sample mounting dock.

This was a fairly simple exercise, using hooks similar to the ones employed on the dock which this time engage only the front transport ring of the sample carrier. In this case there is no need for electrical connectivity to be provided through the hooks and onto the transport ring, so all three hooks contact the single transport ring without the need for them to be staggered or electrically isolated as on the sample dock. Figure 2.6 shows a detail of this design and the available degrees of freedom used when performing sample transfer.
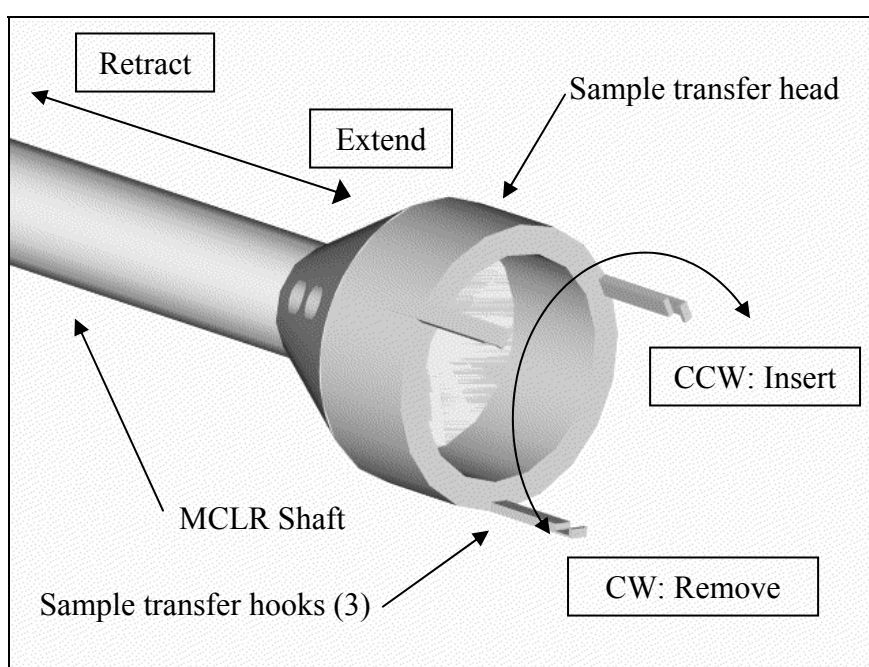
Figure 2.6   Sample transfer tool as installed on MCLR shaft.   Rotary and linear degrees of freedom are utilized for sample transfer as shown.

Design Revision Process

The design went through a major revision near the end of the project when it was discovered that the increased length of the sample from the vertical center of rotation on the original design made it impossible to conduct scattering experiments at significant angles or to clean samples via use of the sputter gun. Accordingly a substantial redesign

took place with the goal of dramatically shortening the overall length of the configuration. This goal was reached via the following changes:

1. Moving the worm gear used to rotate the sample dock from the front of the manipulator head to the back. This then made it possible to move the entire docking system closer to the body of the manipulator.

2. Reducing the thickness of each of the rings on the sample carrier from 1/8" to 1/16" The clearance between successive rings was also reduced from 3/16" to 1/16". These changes required that the docking hooks and alumina spacers between rings had to be modified (shortened) as well.

3. Adding a separate cooling head.

4. Moving the sample holder stack so that it was no longer secured to the front of the sample carrier faceplate, but to the back. The sample is then accessible via a circular aperture in the carrier faceplate. This has the added advantage that it allows us to bring the sample carrier into direct contact with the dock's cylindrical copper body, making cooling more efficient and less likely to adversely effect the fragile insulators used in design of the carrier.

These changes allowed us to reduce the overall distance of the sample from the vertical axis by over 1.1". The original design centered the face of the sample within the scattering chamber. While still leaving the sample 0.66" off center, the changes outlined above are adequate to achieve all likely scattering parameters using X and Y manipulator translations. Since these axes rotate with the sample, the X axis, perpendicular to the face of the sample allows control over the radial distance of the sample from the chamber center. Both the X and Y translation axes allow approximately 0.5" total translation off center in each direction, so by translating along the X axis radially toward the center of the chamber we can reduce the total sample displacement from center from 0.66" to 0.16". To re-align the center of a sample with the center of the beam then requires Y axis translation, along the direction parallel to the sample face, with the translation distance depending on the incident scattering angle parameter. A table of Y axis manipulation values necessary to maintain sample centering for particular incident scattering angles is

presented in Appendix A.

      Fabrication drawings of the various sample holder, dock, and transfer apparatus are available for future reference in the "Sample Transfer System Fabrication Drawings" notebook stored in Lab 13.

CHAPTER 3

ELECTRONICS, INSTRUMENTATION AND INTERFACING

Introduction

A significant portion of the scope of this project involved adding to and/or upgrading the existing instrumentation and electronics capabilities of our experiment. As originally installed the beamline was operated almost exclusively by a wide range of custom-built, manual, analog power supplies and control boxes. This meant that practically any operation on the beamline, even something as simple as tuning a beam or monitoring its stability over time required a large amount of repetitive labor and observation, from the actual tuning operation to monitoring and recording of instrument readings. While some level of manual control is desirable with the system because of the sensitive and temperamental nature of many of the existing beamline instruments and the difficulty and expense that would be required to fully automate most processes, it is desirable to reduce the amount of tedious manual operations required for certain basic, frequent operations such as monitoring of long-term beam stability. To this end a LabView software program was written, integrated, and implemented to give a basic real-time graphical readout (and text-file output capability) of the beam current data obtained via the Keithley 617 GPIB-capable electrometer we use to measure beam intensity at one of the 3 Faraday cup devices on the beamline [18].

In addition to the need to automate repetitive tasks was the need to perform complex or high-speed automated data acquisition processes. Previously this was accomplished by using a GPIB-bus enabled Linux/Unix workstation to interface with

several analog and digital acquisition devices, both off-the-shelf and custom built. These routines involved simultaneous analog to digital conversion, counting, and analog and digital IO using several discrete components. However, upon bringing the system back online it was found that several of the key components from the previous implementation were no longer operational. Additionally, the age of several of the other components, the difficulty of adapting and debugging the legacy C code, and the overall preference for an integrated, graphical interface/virtual instrument approach made it reasonable to simply rewrite these components from scratch using LabView, a highly intuitive yet quite versatile graphical programming language.

The flexibility, usability, and capability of our LabView instrumentation server was greatly enhanced by installation of a high-data rate, multifunction DAQ card (IOTech DaqBoard/1000). Several key programs would have been significantly more difficult to implement without the capabilities provided by this advanced interface.

The remainder of this chapter will be devoted to discussing instrumentation and programming work for the following three systems: 1) current monitoring/electrometer automation; 2) Colutron beam tuning; and 3) electrostatic analyzer (ESA) operation. These projects will be discussed in turn and related to each other where appropriate. They are listed above in order of increasing algorithmic and/or implementational complexity:

Due to the nature of LabView graphical code it is not practical to include the actual code in this document. However, Appendix B includes logic flow charts of the three main programs discussed here for future reference. The appropriate files may be found using the filenames accompanying those charts.

Current Monitoring/Electrometer Automation

During beamline operation it is frequently desirable to obtain some indication of the beam's ion flux. Since the charge state of individual ions is known (this is constrained by Colutron and monochromator tuning), a generalized relationship exists between the current carried by a beam and the flux. This relationship can be quantified as

$$I = \sum_i q_i \Phi_i \qquad (1)$$

where q is the charge state of a particular species i and Φ_i is the species' total flux.

Beam current is measured using Faraday cups installed at strategic positions along the beamline. Coupling these devices with a high-precision digital electrometer (in this case a Keithley 617) produces an instrument capable of measuring the beam flux with a high degree of precision. Since the KE 617 is also programmable via the General Purpose Instrumentation Bus (GPIB/IEEE-488) specification [19], the instrument can be interfaced with a PC to enable real-time monitoring of the beam's behavior, with graph history and the ability to output data files.

There are several circumstances in which a measurement of the behavior of a beam's flux over time would be desired. First, when tuning a beam we desire to maximize the total beam flux into one of the three Faraday cups installed in the different sections of the beamline. The first one, just past the source/Colutron section, is needed to maximize beam flux through the Colutron (magnetic filter) and the first set of electrostatic filters. The second, past the 90° monochromator section, is needed to properly tune the monochromator settings, again with the goal of maximizing beam flux.

The third one is mounted inside the chamber at the bottom of the manipulator head and can be maneuvered into position where the sample would normally sit to maximize final beam flux. Use of an automated program speeds up this tuning process by giving a visual representation of beam flux as the filter parameters are adjusted. Although it is possible to manually adjust the beam flux using the electrometer readout, it is usually more efficient to use an automated program to visualize the maximization process instead.

The second requirement for a beam current monitor is due to the need to monitor beam stability over relatively long periods of time. Because of the natural fluctuation of emitted flux due to source variations, heating effects, etc it is vital that we be able to monitor changes to beam flux to ensure that beam flux at the sample is constant over relatively short time scales, such as the amount of time it would take to acquire a set of scattering measurements. After tuning a beam into the chamber and prior to obtaining scattering measurements it then becomes necessary to monitor beam current into one of the Faraday cups for some period of time to ensure that the beam is relatively stable. This monitoring operation is difficult to do without the aid of a graphical interface showing the beam history. The program also needs to be able to quantitatively calculate a statistical measure of the change in flux over its history since graph scaling issues can sometimes lead to misinterpretation of purely graphical results.

Implementation of the program was fairly straightforward: the program needed to begin a continuous acquisition via GPIB from the Keithley 617 on demand, outputting real-time electrometer data to a history graph while simultaneously calculating the percentage change from the beginning of the acquisition. It should also automatically generate an output data file at the end of each acquisition. This program has been

completed, tested and debugged and is presently in operation. Details of the algorithm employed can be found in the corresponding logic flowchart in Appendix B.

<u>Wien Filter Beam Tuning</u>

One of the first procedures undertaken in preparing a beam for an experiment involves tuning the Wien filter, often referred to as the "Colutron" after its manufacturer. The device consists of a pair of coupled coil electromagnets at right angles to a pair of electrostatic deflectors, all mounted on opposite sides of the first section of the beamline, just past the ion source. Between the electromagnets the magnetic field is approximately linear and is roughly linearly dependent on the coil current. By graphing magnetic field versus coil current for a known source (Rb) we obtained a magnetic field-current relationship of

$$B_0 = 0.022 \, I_{coil} . \tag{2}$$

The electric field between the plates is also linear can be considered to be equal to the voltage difference across the plates divided by their separation. For this system the relationship between voltage and electric field is given by

$$E_0 \cong \left(12\,500/225\,m\right) V_m \tag{3}$$

(based on manufacturer specs of E_0 =12 500 V/m @ 225 V [20]). A general set of differential equations describing the system would be as follows, with the $\bar{z}$ direction the beam's direction of propagation [21].

$$\begin{cases} m\,\ddot{x} = e\,E_x + e\,\dot{z}\,B_y \\ m\,\ddot{y} = e\,E_y - e\,\dot{z}\,B_x \\ m\,\ddot{z} = e\,E_z - e\,\dot{z}\,B_z \end{cases} \tag{4}$$

If we assume the magnetic field to be B_0, directed along the x-axis and

perpendicular to the electric field, E_0, aligned with the y-axis, these differential equations become [22]:

$$\begin{cases} m\ddot{x} = 0 \\ m\ddot{y} = eE_y - e\dot{z}B_x \\ m\ddot{z} = 0 \end{cases} \tag{5}$$

Since the second equation is the only nontrivial one it is obvious that the only net force applied to the beam is in the plane perpendicular to the magnetic field and depends on the velocity $(\dot{z})$ of the beam. Solving for the case of an undeflected beam, where

$$\sum F = m\ddot{y} = 0, \tag{6}$$

we find that only ions satisfying the parameter $\dot{z} = v = E_0/B_0$ will pass through undeflected. Since the kinetic energy of the beam, K, is related to the velocity via

$$K = \tfrac{1}{2}mv^2 = qV \tag{7}$$

where V is the beam voltage and q the ion charge, we can rewrite the above condition as

$$\frac{q}{m} = \frac{1}{2V}\frac{E_0^2}{B_0^2}, \tag{8}$$

so for this case specifying a beam velocity is the same as choosing a particular charge-mass ratio. This makes it clear that operation of the Wien filter introduces a slight ambiguity, since all ions with the same approximate charge-to-mass ratio (velocity) will be passed through, so the Wien filter does not specify the beam parameters as uniquely as might be desired. In practice, this can be a significant problem for certain types of beam containing high impurity ratios, especially when the impurities exist in multiply-charged states and significantly different atomic mass. This difficulty is resolved by concurrent use of a 90-degree spherical electrostatic analyzer as a monochromator. This device is

designed such that it passes only particles of a precise energy, E_{pass}, such that

$$V_{sphere} = E_{pass}\left(\Delta r \middle/ r_m\right) \tag{9}$$

[23], thus eliminating the ambiguity. The monochromator is designed such that $\Delta E / E \cong 1\%$, so the Wien filter and monochromator together give us a very clean, precisely specified beam.

Because of its ability to pass ions of only a selected *q/m* ratio, the Wien filter is just as useful for isolating the desired beam current out of the background of various isotopes, charge states, and atomic species present in commercially available ion sources as it is for maximizing beam current. Although for some source types, such as aluminosilicate solid-state sources, this background is relatively minimal, other types, particularly gas sources, often generate a fairly "dirty" beam which would be impossible to purify without a device of this type. In any case, even the purest beam emitter sources contain at least some isotopic impurities which it would be desirable to filter out before the scattering section, making the Wien filter a necessary component of a "clean" experiment.

The process of tuning a beam through the Wien filter requires the operator to cycle through a range of magnet current values while recording the corresponding beam current values in the Faraday cup mounted just past the Colutron section. Unfortunately, the process of cycling the magnets while monitoring beam current becomes very tedious and time-consuming. Since the process is easily automated given a relatively small set of arbitrary initial parameters a LabView program was written to carry out this task automatically. (Note that this program is operational, but as the first major program written for this project is in need of some modification to achieve optimal operation.)

This program required simultaneous GPIB access to two channels: first, the channel used by the Kenwood PD36-20AD/GP-610D power supply controlling the Wien filter magnet current [24] and second, the channel used to obtain beam current data from the ubiquitous KE617 electrometer.

The algorithm for this program is more difficult due to the large number of input variables. The program needed to be able to increment either automatically (timed) or manually through a set of data points which the program calculates using a set of input parameters for initial and final current values and current step increment. It should pause after switching current values but before reading the corresponding electrometer value by an amount of time given by a delay time control, which allows the change in beam parameters to catch up before a reading is taken. Once it reaches the peak value the program then needs to be able to gradually ramp down since a sudden increase or decrease of current may be harmful to the Wien filter magnets. Peripheral functions also desired include a built-in calculator to calculate peak mass based on the corresponding input parameters and the ability to zero or un-zero the electrometer on demand.

The logical design of this program is likewise given in the corresponding flowchart figure in Appendix B.

<div align="center">Electrostatic Analyzer Automation</div>

During a scattering experiment the most basic piece of experimental data is the range of scattered intensities for the particular incident angle. To obtain this data we use a hemispherical electrostatic analyzer, or ESA. The central component of the ESA is an electron-multiplier detection unit, mounted in the plane of the beam and rotateable to be able to intercept ions scattered from the sample at a wide range of angles. This allows us

to obtain beam intensity values for whatever needed. Typically the sample is set at some standard incident angle θ_i to the beam (i.e. 30°, 45°, 60°, etc) and the ESA detector is rotated through a spectrum of scattered angles θ_f giving a spectrum of angular intensity information for a particular incident angle.

The actual data generated by the ESA comes from the electron multiplier but is first processed by a Modern Instrumentation Technology (MIT) F-100T preamplifier, which amplifies the electron multiplier signal and generates a corresponding binary signal from the analog input based on a built-in discriminator level. The preamp output signal is then measured by a counter, which generates frequency or totalized counting information as required.

Taking ESA data requires a software solution, since the scanning needs to take place at higher rates than possible for manual acquisition. The previous solution consisted of PC interfaced with a custom-built DAC board (which generated programming voltages) and also, via GPIB, with a HP5335A counter. The PC's C++ program used the DAC board to sequentially generate programming voltages while simultaneously monitoring the counter output over GPIB. Unfortunately the DAC board, which had a history of unreliability, failed again, leaving the necessity of replacing it with something more reliable. In addition, the age of the equipment, the difficulty of maintaining the code, and the desire for more graphical, real-time feedback results made it reasonable to scrap the previous system altogether. Rather than replacing the failed components an IOTech DaqBoard/1000 LabView-capable PCI interface card was acquired. The multiple previous components and custom-built electronics could then be abstracted to graphical, modular LabView code, simultaneously giving greater code

flexibility and more transparent operation.

The design process for this program was convoluted. The first major issue encountered was due to the difficulty of setting up even a simple acquisition or output using IOTech's supplied LabView code library. Unfortunately the design of these components was quite non-intuitive and required several poorly-documented steps to obtain the desired results. Nevertheless, these issues were eventually overcome and the algorithm design stage completed.

Because of IOTech's peculiar LabView implementation the first step to be taken at the beginning of an acquisition was to initialize the DAQ board by inputting the relevant channel and I/O information. Subsequently the program would begin cycling through pass energy values using the starting and final energy values supplied and dividing the energy bandwidth by the number of desired points. For a given pass energy value the program calculates the necessary power supply programming voltage for the power supply being used (either the low- or hyperthermal-energy ESA power supply) using a formula derived from manual calibration of the supply. It then writes that programming voltage to the power supply, which sets the ESA sphere voltage as desired and specifies the pass energy. The program then waits for a period of time specified as the sleep time before beginning to record counts.

Another major hurdle was encountered in the process of attempting to obtain ESA counts using the TTL counter channel on the IOTech board. Since the F-100T preamp apparently outputs a voltage well below standard TTL-high levels the initial assumption was that the signal needed to be amplified. However, testing of various op-amp, discriminator, and trigger circuits never showed capability to do anything other than

amplify the noise background.   Meanwhile the HP 5335A counter used previously worked fine as long as the trigger level was set low enough to trigger off the reduced-amplitude preamp signal.   Deeper investigation showed that while the HP counter is capable of measuring signals with frequency of up to 200 MHz [25], our IOTech Daqboard/1000 was limited to 200 kHz [26].   Although the counting rate was only approximately 1 kHz, the extremely short pulse length (~10 ns) made the necessary *effective* sampling rate approximately 100 MHz.   Since the DAQ board clearly was unsuitable for this application it was decided to revert to using the HP 5335A counter for sampling while continuing to use the DAQ board to output voltage values to the power supplies.

Returning to the algorithm execution narrative, the HP counter will be instructed using GPIB to collect data for a precisely defined time window, which the program refers to as dwell time.   At the end of that time a GPIB read command returns the collected number of counts to the program, which stores the data in an array and displays it on a graph showing the data for the current sweep.   The program then increments the pass energy and continues to take successive detector counts vs. pass energy data until it reaches the end of the acquisition.   Once data acquisition is complete the program takes the necessary steps to properly close the DAQ interface.   The user then has the opportunity to save an output file of the acquired data.

This program is functional but still in the testing stage.   Just as the issues with the DAQ counter operation were not apparent until the program could be tested with a real signal it is likely that other bugs will be encountered under increasingly realistic testing scenarios.   Nevertheless, the basic program algorithm as shown in the corresponding

logic flowchart in Appendix B will likely remain basically unchanged.

Conclusion

This thesis has been devoted to discussing changes to the Sosolik Group ion beamline instrument necessary to accomplish a new class of experiments extending previous Schottky diode chemicurrent measurements to hyperthermal- and low-energies using an accelerated ion beam. The previous experiments are discussed and the results likely to be observed using the different experimental parameters are evaluated. The final chapters discuss the scope of work involved to enable these measurements to be taken, with separate chapters devoted to changes made in the areas of apparatus and instrumentation design, respectively.

APPENDICES

Appendix A

Table of Manipulator Centering Values by Angle

Table A.1 Required Y-axis manipulator values for re-centering of manipulator. All dimensions given are relative to the center of the scattering chamber. For negative angles use reciprocal Y values.

Incident Angle, θ_i [°]	Y position [in.]
10.0	0.028
15.0	0.044
20.0	0.058
25.0	0.075
30.0	0.092
35.0	0.112
40.0	0.134
45.0	0.160
50.0	0.191
55.0	0.229
60.0	0.277
65.0	0.311
70.0	0.440

Appendix B

Logic Flow Diagrams of LabView Programs
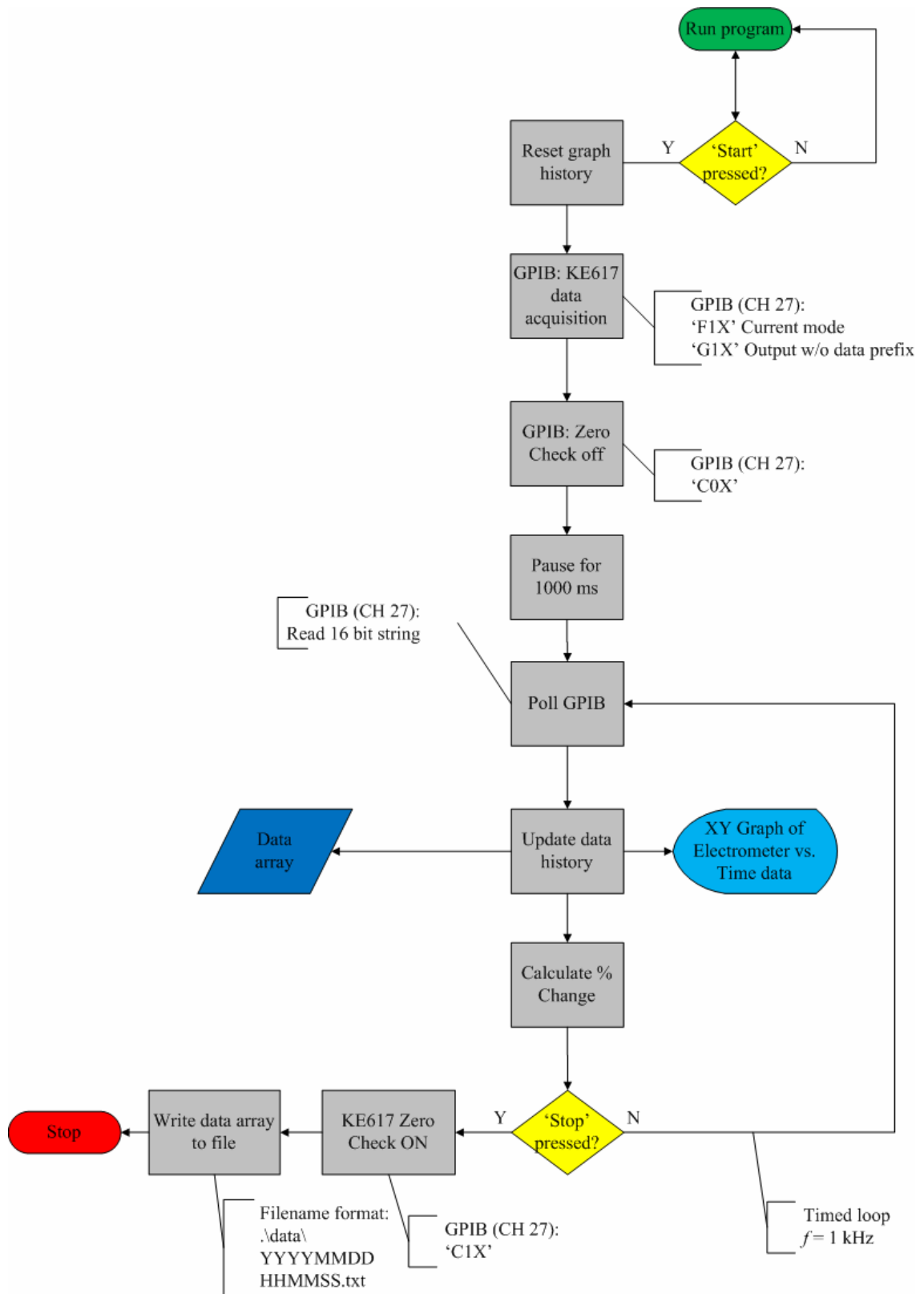
Figure B.1   Logic flow diagram corresponding to LabView code for Keithley 617 electrometer monitoring .   Appropriate GPIB commands for the KE 617 are shown.
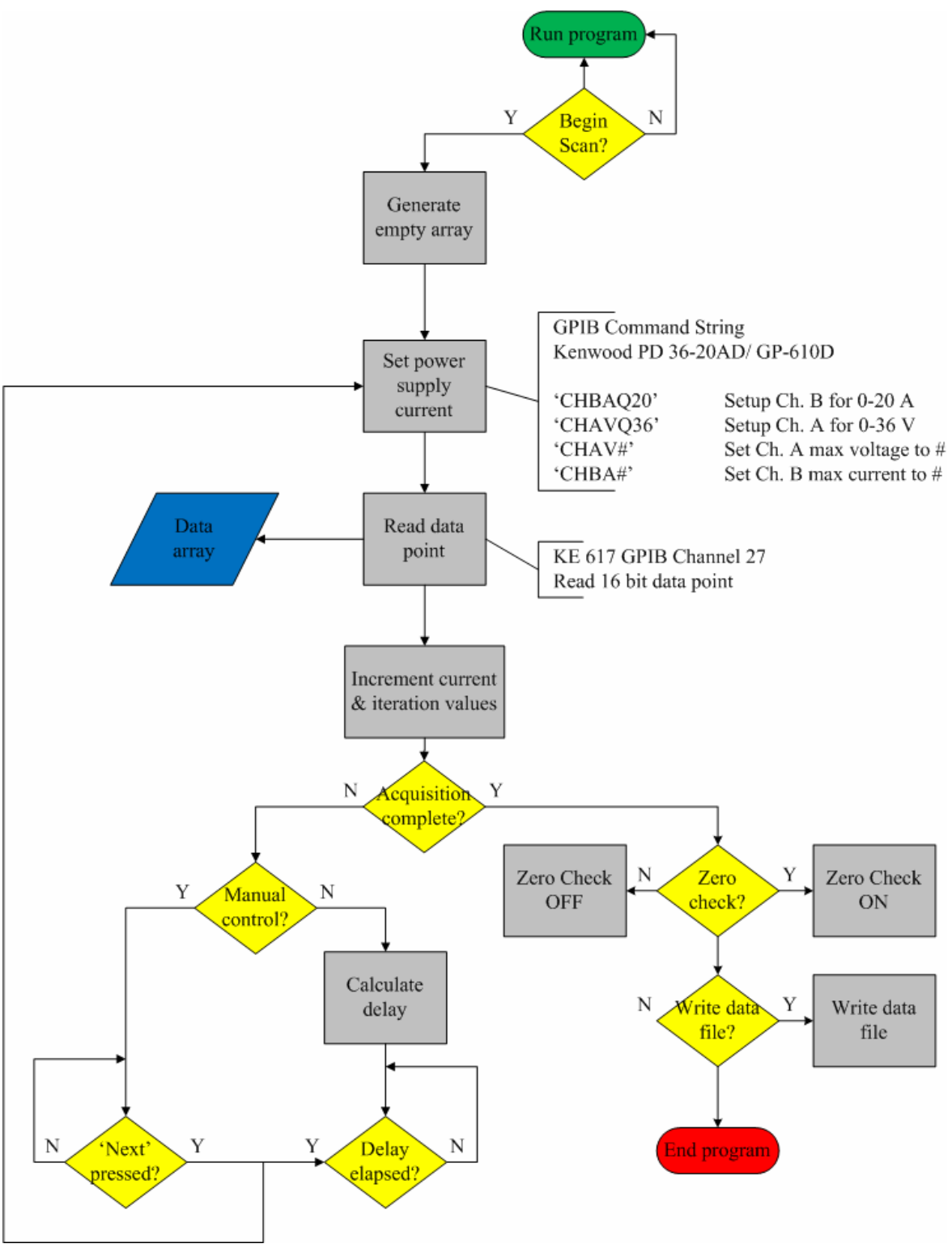
Figure B.2   B.2   Logic flow diagram corresponding to LabView code for Wien filter automation. The necessary GPIB commands for both the KE617 and Kenwood PD36-20AD are shown.
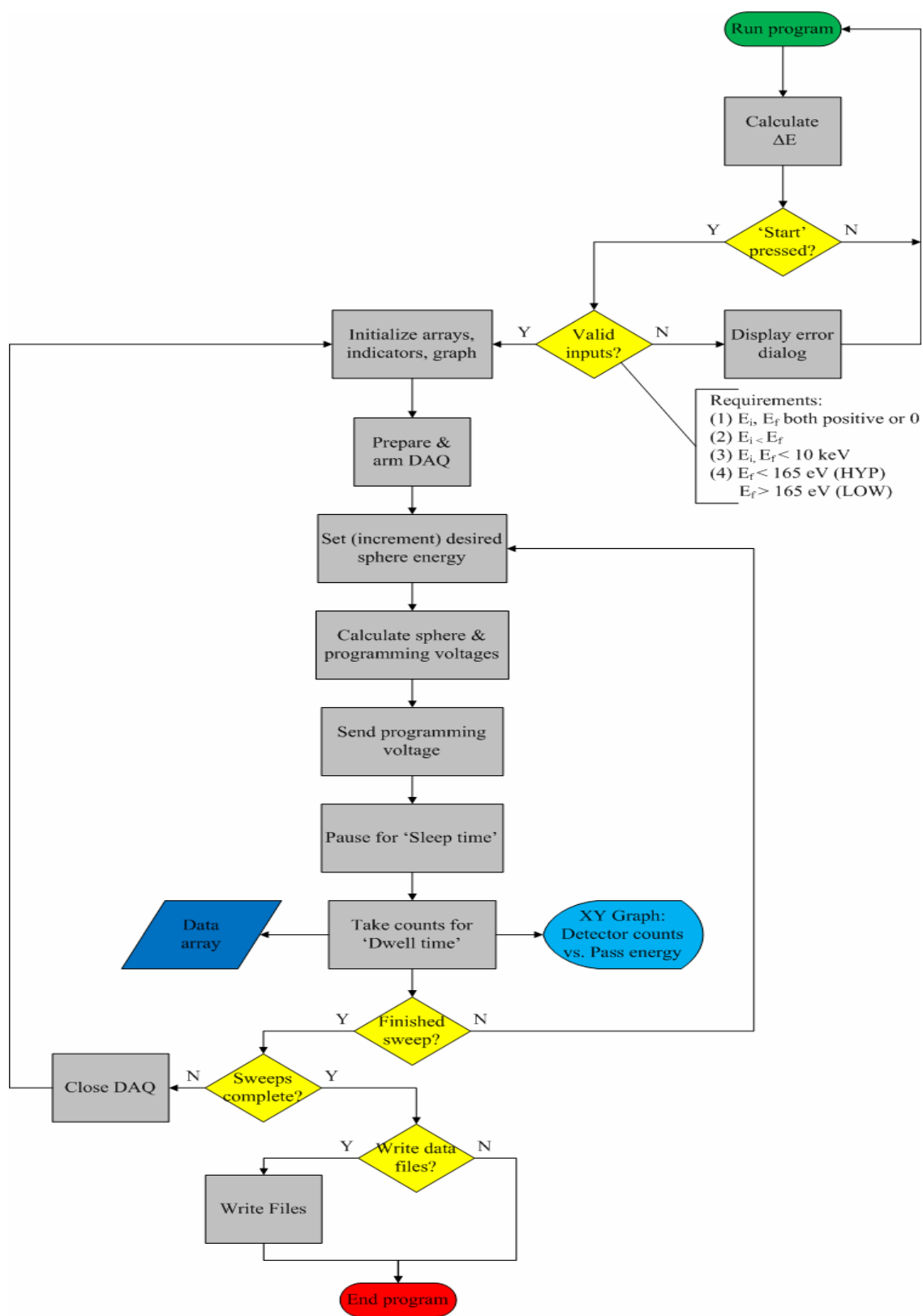
Figure B.3   Logic flow diagram corresponding to LabView code for electrostatic analyzer (ESA) automation.

REFERENCES

1. D. L. Adler *Kinematics of Hyperthermal Energy Ion Scattering* (Cornell University: Dissertation) (1989) 11.

2. C. E. Sosolik *Heavy Atom Collisions and Thermal Effects in Hyperthermal Energy Ion-Surface Scattering* (Cornell University: Dissertation) (2001) 4.

3. R. L. McEachern *Trajectory and Impact Parameter Analysis of Hyperthermal Ion Scattering* (Cornell University: Dissertation) (1990) 22.

4. R. L. Seliger *J. Appl. Phys* **43** 5 2352-57 (1972).

5. Adler 23-28.

6. Adler 15.

7. Adler 17-22.

8. Adapted from H. Nienhaus *Surf. Sci. Rep.* **45** 5 (2002).

9. H. Nienhaus *Phys. Rev. Lett.* **82** 446- 449 (1999).

10. H. Nienhaus *Appl. Phys. Lett.* **74** 4046-4048 (1999).

11. Adapted from H. Nienhaus *Phys. Rev. Lett.* **82** 446 (1999).

12. Adapted from H. Nienhaus *Phys. Rev. Lett.* **82** 446 (1999).

13. H. Nienhaus *Phys. Rev. Lett.* **82** 447 (1999).

14. H. Nienhaus *Phys. Rev. Lett.* **82** 447 (1999).

15. McEachern 17-18.

16. McEachern 29.

17. J. H. Moore, C. C. Davis, and M. A. Coplan *Building Scientific Apparatus* (Cambridge[Mass.]: Perseus Books) (2003) 105.

18. McEachern 24.

19. *Model 617 Programmable Electrometer: Quick Reference Guide* (Cleveland: Keithley Instruments) (1984) 35.

20. http://www.colutron.com/products/kit/sample.html

21. Seliger 2352.

22. Seliger 2352.

23. Adler 24.

24. *GP-610A/GP-610D GP-IB Adapter Instruction Manual* (Yokohama [Japan]: Kenwood TMI Corp.).

25   *Operating and Service Manual; 5335A Universal Frequency Counter* (Santa Clara: Hewlett Packard Co.) (1980) 1-2.

26   *DaqBoard/1000 and /2000 Series User's Manual* (Cleveland: IOTech Inc.) (2005) 1-2.